Assessing shoreline dynamics over multiple scales on the northern Yucatan Peninsula

Torres-Freyermuth, Alec; López-Ramade, Eduardo; Medellín, Gabriela; Arriaga, Jaime A.; Franklin, Gemma L.; Salles, Paulo; Uribe, Abigail; Appendini, Christian M.

DOI
10.1016/j.rsma.2023.103247

Publication date
2023

Document Version
Final published version

Published in
Regional Studies in Marine Science

Citation (APA)
Torres-Freyermuth, A., López-Ramade, E., Medellín, G., Arriaga, J. A., Franklin, G. L., Salles, P., Uribe, A., & Appendini, C. M. (2023). Assessing shoreline dynamics over multiple scales on the northern Yucatan Peninsula. *Regional Studies in Marine Science*, *68*, Article 103247. https://doi.org/10.1016/j.rsma.2023.103247

Regional Studies in Marine Science 68 (2023) 103247

Contents lists available at ScienceDirect

Regional Studies in Marine Science

journal homepage: www.elsevier.com/locate/rsma

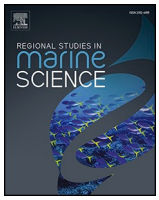

Assessing shoreline dynamics over multiple scales on the northern Yucatan Peninsula

Alec Torres-Freyermuth [a,*], Eduardo López-Ramade [a], Gabriela Medellín [a], Jaime A. Arriaga [b], Gemma L. Franklin [a], Paulo Salles [a], Abigail Uribe [a], Christian M. Appendini [a]

[a] Laboratorio de Ingeniería y Procesos Costeros, Instituto de Ingeniería, Universidad Nacional Autónoma de México, Sisal, Yucatán 97385, Mexico
[b] Faculty of Civil Engineering and Geosciences, Delft University of Technology, 2628 CN Delft, the Netherlands

ARTICLE INFO

Keywords:
Shoreline
CoastSat
AVISO++
Copernicus
Beach erosion
Sand waves

ABSTRACT

Coastal erosion is critical in many locations along the northern Yucatan Peninsula. The area is characterized by a micro-tidal regime and low-energy wave conditions, with a high-incidence angle with respect to the shoreline. Port and harbor infrastructure for fisheries, commercial, and tourist activities has promoted the growth of coastal communities settled on barrier islands. However, the human settlements have degraded the coastal ecosystems and interrupted the littoral transport. Due to coastal development in the region, the land use of the remaining pristine coastal areas is expected to change in forthcoming years. Thus, understanding coastal changes occurring along the northern Yucatan Peninsula is fundamental for improving coastal planning. We employed open access remote sensing data sets and reanalysis information to investigate shoreline changes at different spatial and temporal scales. Shoreline position was obtained along a 150-km stretch of coast from satellite imagery using CoastSat. Firstly, reanalysis and satellite-derived information were validated with in situ measurements in the vicinity of coastal structures. A satisfactory agreement was found for characterizing the forcing conditions (waves and sea level) and shoreline evolution at different temporal scales. A dominant direction of alongshore sediment transport (50,000–80,000 m^3/year) make the shoreline highly sensitive to any nearshore disturbance. We found that coastal erosion occurred in 50% of the analyzed transects, whereas beach accretion occurred in only 30%, suggesting net beach losses. Erosive trends are strongly correlated with the presence of coastal structures. The 6-km long Progreso pier induced significant beach erosion along $O(10)$ km, while sheltered harbors induced downdrift erosion along $O(1)$ km. Detached breakwaters and groins have an overall negative impact on downdrift areas ($O(100)$ m). On the other hand, significant erosion was also observed in pristine areas located downdrift of a coastal lagoon due to the sediment impoundment associated with the growth of a sand spit. Moreover, shoreline sand waves drive 40-m shoreline oscillations and propagate (alongshore) at a rate of 300 m/year. The generation of sand waves seems to be related to both natural and anthropogenic perturbations, in combination with the high-incidence wave angle. Their propagation plays a key role in the shoreline dynamics of this region.

1. Introduction

The morphology of sandy beaches undergoes continuous changes associated with the interaction between wind, tides, waves, and currents (Aubrey, 1979; Wright and Short, 1984). This natural response is affected by man-made structures, such as breakwaters, geotextiles, groins, ports, and navigation channels among others, as they interrupt cross-shore and alongshore sediment transport (Komar, 1998; Williams, 1999; Turner, 2006; Ratnayake et al., 2018), in addition to modifying currents with the potential to produce sediment transport gradients (Ranasinghe and Turner, 2006; Pattiaratchi et al., 2009). Moreover, climate change can further exacerbate coastal inundation and beach erosion due to sea level rise and increased intensity and frequency of storms (Ranasinghe, 2016).

Beach morphology varies at different spatial and temporal scales (Zenkovich, 1967; Coco and Murray, 2007). In the short-term, storms can produce extensive erosion over a scale of hours, causing dunes to collapse (De Winter et al., 2014), the shoreline position to retreat, and

* Corresponding author.
E-mail address: atorresf@iingen.unam.mx (A. Torres-Freyermuth).

https://doi.org/10.1016/j.rsma.2023.103247
Received 29 June 2023; Received in revised form 8 October 2023; Accepted 14 October 2023
Available online 19 October 2023

moving sandbars farther offshore (Sallenger et al., 1985; Gallagher et al., 1998; Hoefel and Elgar, 2003; Vidal-Ruiz and Ruiz de Alegría-Arzaburu, 2019). A strong storm sequence could even surpass expected decadal erosion associated with sea-level rise (Harley et al., 2022). In the medium-term, beach morphology can change due to seasonal variations in the forcing, as the beach slope is modified and the shoreline reconfigured (e.g., beach rotation, see Ojeda and Guillen, 2008; Ruiz de Alegria-Arzaburu and Masselink, 2010; Harley et al., 2015). On a longer time-scale, wave climate variability associated with the ENSO can induce interannual variability in beach morphology (Mortlock and Goodwin, 2016; Barnard et al., 2017; Almar et al., 2023), whereas in the long-term shoreline changes can be related to sea-level rise (Ranasinghe et al., 2012) or sediment transport gradients (e.g., Appendini et al., 2012). The latter is particularly evident along coasts with a clearly dominant direction of alongshore sediment transport as the affected area can occur several kilometers downdrift of an anthropogenic intervention (Williams, 1999).

Shorelines can present undulating shapes associated with kilometer-scale sand waves (Ashton et al., 2001; Falqués, 2006; Medellín et al., 2008). These morphological features often present spatial scales (i.e., characteristic wave length) on the order of 2–5 km and migration rates of 100–300 m/year (Guillen et al., 1999). Sand waves can grow and migrate downdrift, depending on advective and diffusive sediment fluxes, providing a massive sediment addition to the coastal system (e.g., Warrick et al., 2023). Downdrift migration of sand waves drives a temporal variation in the shoreline position characterized by an accretional downdrift end and an erosional updrift end, with beach width difference of 50–100 m (Davidson-Arnott and Van Heyningen, 2003). Thus, they are also referred to in the literature as accretion/erosion waves (Inman and Bagnold, 1963). Nevertheless, large-scale sand waves' role in coastal dynamics is often ignored in coastal planning.

Given the multiple processes and scales involved in the complex beach response, it is crucial to understand the beach evolution at a regional scale (O~100 km) for the integral planning of the coast. Fortunately, the advent of satellite imagery (Garcia-Rubio et al., 2015; Vos et al., 2019; Nidhinarangkoon et al., 2023; Vitousek et al., 2023; Westley et al., 2023; Amalan et al., 2018) allows coastal dynamics to be investigated over large areas, serving as the sole source of information in regions where in-situ data is scarce. Satellite imagery in coastal engineering studies has increased exponentially over the past decade (Turner et al., 2019). Vos et al. (2019) developed an open-source software (CoastSat) to analyze shoreline evolution from publicly available Google Earth Engine imagery. The satellite-derived shoreline position obtained with CoastSat has been widely validated in different coastal settings (e.g., Vos et al., 2019; Castelle et al., 2021; among many others).

The northern Yucatan Peninsula coast is a low-lying area prone to winter and tropical storms. Furthermore, this region presents a persistent littoral transport (Appendini et al., 2012). Prior field observations have been obtained on a few field sites due to the challenges of covering extended locations. Hence, they have mainly focused on the vicinity of coastal structures to investigate seasonal (Medellín and Torres-Freyermuth, 2019) and short-term (Medellin et al., 2018; Torres-Freyermuth et al., 2019) impacts of coastal structures on beach morphodynamics. However, understanding long-term and interannual shoreline variability is also important at pristine areas in the context of coastal population settlements growth and climate change. A prior study, using remote sensing information, analyzed the shoreline evolution over 20 years only in the vicinity of ports (see Franklin et al., 2021). Moreover, Ruiz-Beltran et al. (2019) conducted a study along 50-km of coast based on 10-years of SPOT-5 images. They reported an unexpected shoreline erosion/accretion pattern in pristine areas without providing a plausible explanation. Thus, the present work aims to fill the existing gap in understanding the role of both natural and anthropogenic perturbations in the interannual and long-term shoreline changes in this region (O(100) km). The present approach, based on remote sensing data and reanalysis information, is valuable at locations in the Global South, where coastal monitoring programs are scarce and are more prone to climate change impacts (Ngcamu, 2023). The multi-yearly shoreline analysis allows us to investigate the role of sand waves on regional shoreline variability. These morphological features can also be important in other regions with significant net alongshore transport.

2. Study area

The study site is located in a low-lying area on the Yucatan coast (Mexico). It comprises approximately 150-km of coast in the northwestern region of the Yucatan Peninsula, from Celestun to Telchac (Fig. 1), characterized by sandy beaches along a barrier island. The sediment is mainly medium to fine sands (Mendoza et al., 2013) of biogenic origin, where skeletal grains and mollusks dominate the sediment composition (Neal et al., 2021). The wave energy is relatively low (H_s< 1 m) due to the wide and shallow continental shelf (slope 1–1000) and the semi-enclosed nature of the Gulf of Mexico. Micro-tidal conditions, with diurnal variations, result in a 0.7 m spring tidal range (Valle-Levinson et al., 2011). The net alongshore sediment transport is westward directed (Appendini et al., 2012) due to the persistent NE winds associated with sea breezes and trade winds (Figueroa-Espinoza et al., 2014). Anticyclonic cold fronts, known as Central American Cold Surges or locally known as *Nortes*, can reverse the alongshore sediment transport (Medellín and Torres-Freyermuth, 2019) and induce significant cross-shore sediment transport (Roberts Briggs et al., 2020). They can also supply sand to the subaerial beach that becomes available for aeolian sediment transport, generating foredune growth. Macrophyte wracks are ubiquitous in the region, showing spatio-temporal variability along the northern Yucatan coast (Ocaña et al., 2023). Although further studies are needed, some works suggest that climate variability (e.g., El Niño) increases the occurrence of *Nortes* in this region (Reding, 1992; Medellín and Torres-Freyermuth, 2019; Odériz et al., 2020). On a longer time-scale, the most important climate change effects are related to sea level rise. *In situ* information and analysis of the mean sea level anomaly from altimetry data suggest an increase of 3 mm/year.

Development along the coast of Yucatan was accelerated with the production of henequen fiber (known worldwide as Sisal) in the early 19th century (Paré and Fraga, 1994), Sisal being the most important port. However, the proximity between the town of Progreso and the state's capital (Mérida) led to the construction of a railroad and a port in Progreso to replace Sisal as the main port for exporting henequen in the late 19th century (Meyer-Arendt, 1993). Following the development of the port of Progreso during the 20th century, the use of beaches to the east and west of the port made it an important destination for local population recreation (Meyer-Arendt, 1987). The construction of eleven small shelter ports along the Yucatan coast in the late 20th century increased coastal development. This development has intensified in recent decades, which has led to an increase of 261% in the coverage area of human settlements (INEGI, 2001; INEGI, 2021). Moreover, the coast's attraction to national and regional tourists has also increased, which has promoted urban development, mainly towards the northeast, primarily between Chuburna and Telchac (Fig. 1e-f).

3. Methods

We employed reanalysis data and remote sensing imagery to characterize the study area and assess shoreline changes along the 150-km coast. The data sources and analyses are described below.

3.1. In situ data

In situ data were obtained to validate reanalysis and remote sensing information. Field observations were mainly collected near the port of Sisal (Fig. 1). Offshore wave conditions were measured with an Acoustic Doppler Current Profiler (ADCP) located 10-km offshore at 10-m water depth (21°16'28.48" N, 90° 3'2.71"W) over the past 10-years.

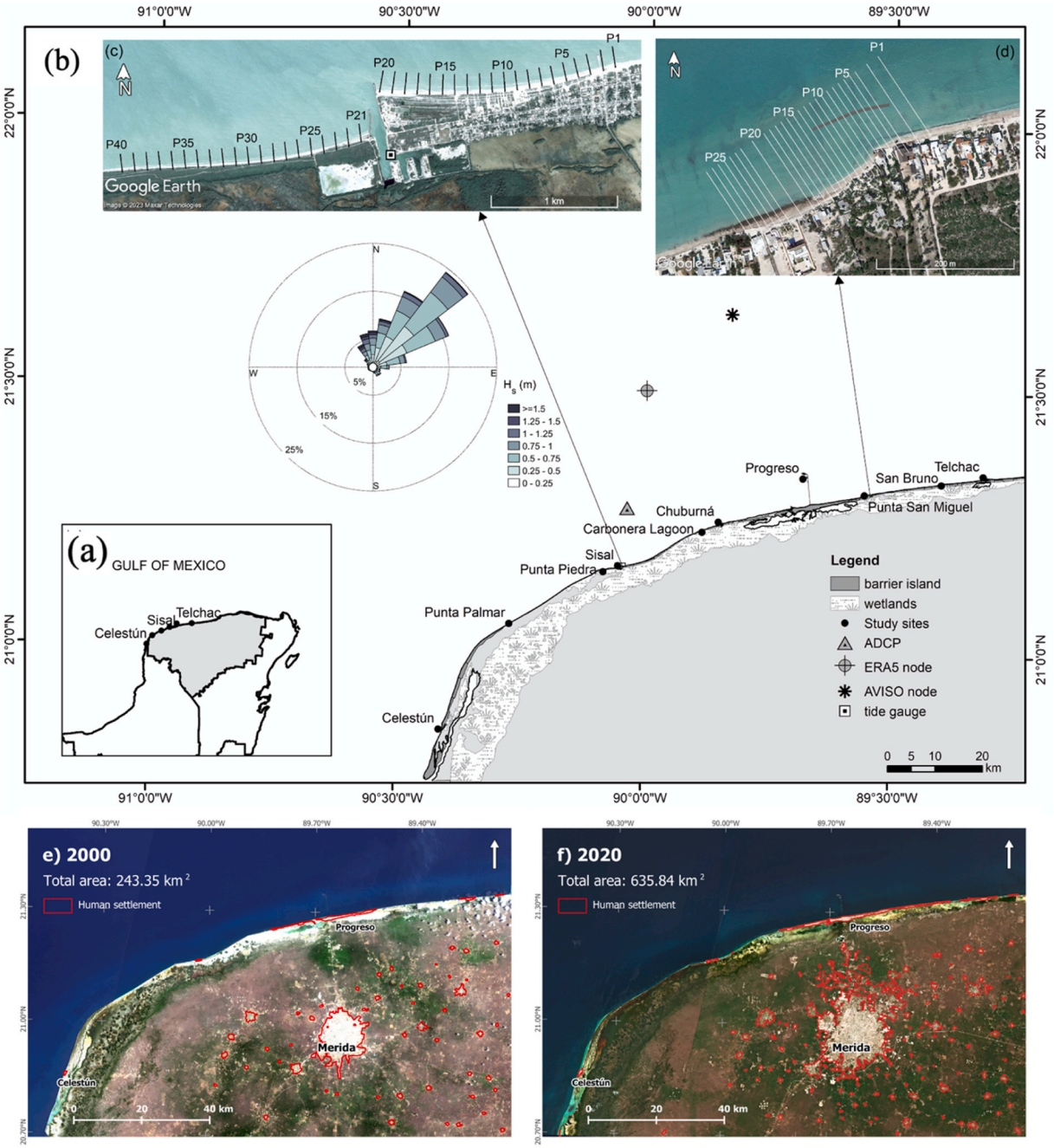

Fig. 1. Location map showing (a) the Yucatan Peninsula in the southeastern Gulf of Mexico, (b) the analyzed coastal section from Celestún to Telchac, and the measured beach profiles used for validation at (c) Sisal and (d) Punta San Miguel (the thick gray line represents the geotube breakwater). True Color Composites with Polygons of "Human Settlement" in red. (e) Three Landsat 7-ETM+ images acquired during April 2000 (courtesy of the U.S. Geological Survey). Polygons of "Human Settlement" in 2000 were defined by INEGI (INEGI, 2001). (f) Three Sentinel 2-MSI images acquired between March and May 2023 (Modified Copernicus Sentinel data 2023/Sentinel Hub). Polygons of "Human Settlements" in 2020 were defined by INEGI (INEGI, 2021).

Significant wave height, mean wave direction, and peak wave period were employed to characterize the wave climate (Fig. 2a). Mean water level has been measured inside the Sisal port with an ultrasonic tide gauge since 2013 (Fig. 1c). Beach profiles were measured every other week east (2015-present) and west (2019-present) of Sisal port (Fig. 1c) using Differential GPS with Real Time Kinematics. A permanent reference station was used, and surveys are taken along 40 cross-shore transects every 100 m, covering from the foredune to a water depth of approximately 1.5 m. The data is referenced to the geoid MEX97, which is a proxy of the mean sea level at this location (Medellín and Torres-Freyermuth, 2019). Moreover, beach surveys from a densely urbanized area (Fig. 1d) were undertaken in 2017–2018 to assess the performance of a detached breakwater (Torres-Freyermuth et al., 2019). This information was also employed in the present study to evaluate the capacity of assessing shoreline changes in the short-term using satellite imagery. Beach profiles were used to track the shoreline position by identifying the cross-shore location where the profile intersects the mean sea level (i.e., $z = 0$ m). The shoreline location from the first survey was subtracted from subsequent surveys to estimate the shoreline position change (e.g., Fig. 2c-d). Hence, negative and positive sign correspond to shoreline erosion and accretion with respect to the first survey, respectively. A thorough description of the methodology

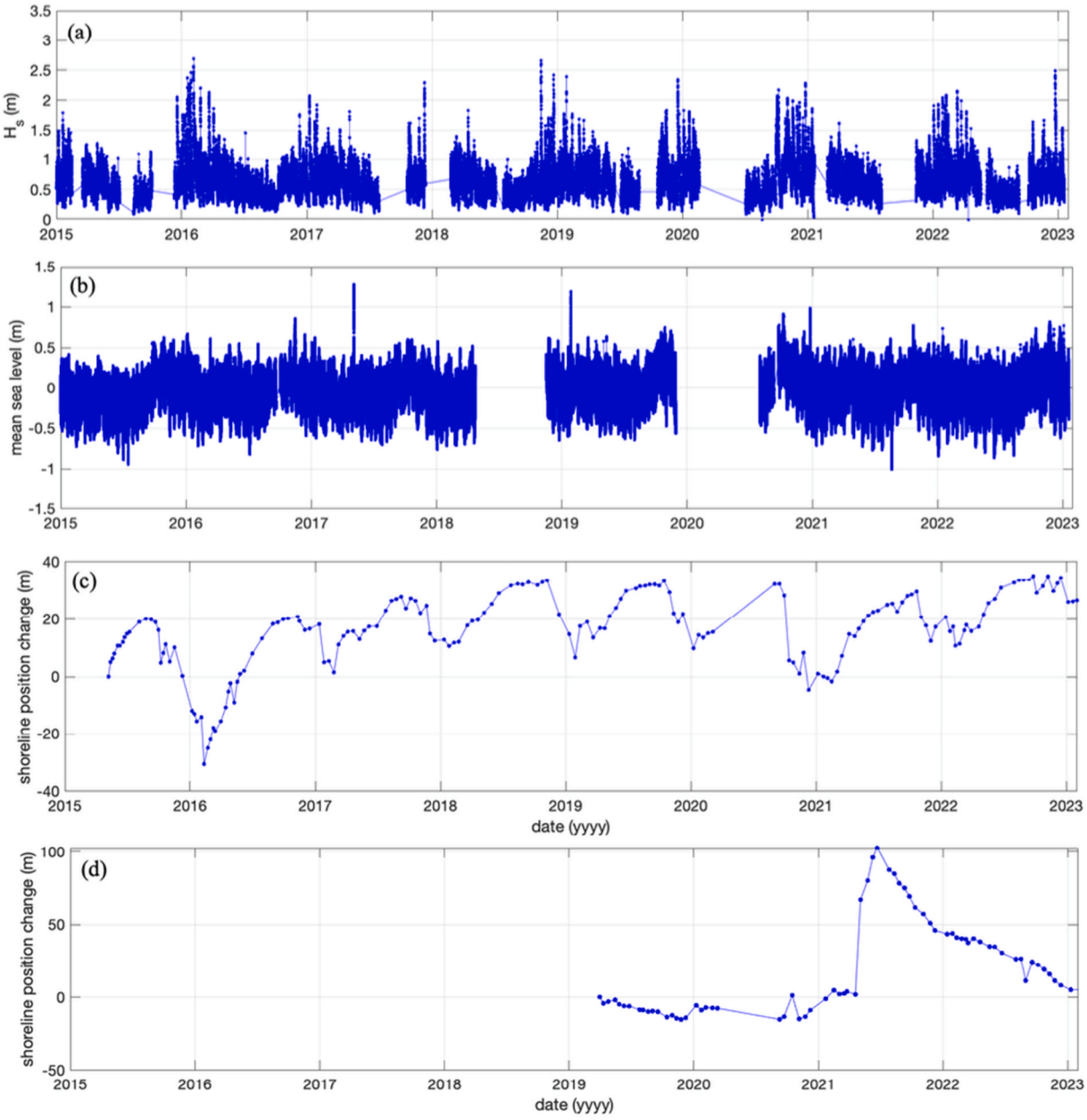

Fig. 2. Measured (a) wave height, (b) mean water level, and shoreline position change at transects (c) P20 and (d) P21.

employed to measure the beach profiles is described in Medellín and Torres-Freyermuth (2019).

3.2. Reanalysis data

To characterize the waves, we employed the ERA-5 reanalysis (https://www.ecmwf.int/en/forecasts/dataset/ecmwf-reanalysis-v5), where the significant wave height, peak wave period, and mean wave direction are validated with in situ ADCP data. In general, the reanalysis data overestimates the wave energy. However, the seasonal variability is well captured, and hence the monthly average of H_s and T_p, and the mode of the mean wave angles were calculated for each year. Subsequently, the mean value for all years and the standard deviation are estimated.

3.3. Satellite data

3.3.1. Sea level anomaly

Satellite altimetry was employed to estimate the sea level change during the analyzed period. The monthly sea level anomaly from altimetry AVISO+ data from 1993 to 2022 was used (http://marine.copernicus.eu/). The data were produced as the Delayed Time Level-4 monthly mean of the sea level anomaly from multi-satellite observations over the Global Ocean referenced to the [1993,2012] period with a 0.25° x 0.25° resolution.

3.3.2. Shoreline position

The analysis of shoreline dynamics on a regional scale was addressed with satellite imagery. This technique has become popular in coastal engineering applications during the last decade (Turner et al., 2019; Ratnayake et al., 2019). The open-access software *CoastSat* (https://github.com/kvos/CoastSat; Vos et al., 2019) was employed for the image acquisition and analysis (e.g., Gunasinghe et al., 2022). The software

includes an algorithm to extract the shoreline position using Machine Learning. This study employed images from the satellite missions Landsat 5 (1986–2011), Landsat 8 (2013–2021) and Sentinel-2 (2016–2021). The temporal and spatial resolution varies from 16 to 5 days and 30–10 m, respectively. The study area was divided into 26 sections for downloading the data, with transects located every 10 m Therefore, time series of shoreline position change were extracted from cross-shore transects at 14,000 alongshore locations. Tidal correction, relaying on beach slope information, was not used in this work. A sensitivity analysis conducted in Sisal shows no significant difference when including the tidal correction, due to the low-energy and micro-tidal regime.

3.4. Data analysis

3.4.1. Sediment transport parameters

Wind waves are the main driver of coastal currents and are responsible for sediment transport near the shoreline. The widely employed CERC formula can be used to compute the alongshore sediment transport. A reformulated expression in terms of deep-water wave parameters was utilized here (Ashton and Murray, 2006; Warrick et al., 2023),

$$Q_s = A_t K_{d50} K_2 H_0^{2.4} T_0^{0.2} \cos^{1.2}(\phi_0 - \theta) \sin(\phi_0 - \theta)$$

where ϕ_0 is the deep-water wave crest angle, θ is the shoreline orientation with respect to the north, A_t is a temporal conversion factor, $K_{d50} = 1$ is an empirical dimensionless scaling factor, and the transport coefficient K_2 is given by,

$$K_2 = \left(\frac{\sqrt{g\gamma}}{2\pi}\right)^{0.2} K_1$$

where the empirical constant $K_1 = 0.4\ \mathrm{m}^{0.5}/\mathrm{s}$. The Q_s was computed for the 2015–2022 period considering different shoreline orientation angles. Subsequently, the annual net alongshore sediment transport was computed for each year and the average and standard deviation of the Q_s net estimates were computed for different shoreline orientations θ.

3.4.2. Shoreline changes

To investigate the spatial-temporal shoreline evolution, a Principal Component Analysis (PCA) was performed at a selected location (e.g., Aubrey, 1979). The temporal and spatial modes of shoreline variability were obtained as,

$$x(y,t) = \sum_{n=1}^{N} c_n(t) e_n(y) \quad (1)$$

where the spatial, $e_n(y)$ and temporal, $c_n(t)$, eigenfunctions were evaluated at each along-shore location, y, and time, t, where the variance decreases with the mode number, n. This analysis has been employed in previous coastal studies to investigate shoreline changes (Medellín et al., 2008; Hansen and Barnard, 2010; Harley et al., 2011). Furthermore, the shoreline rate of change (m/year) at each transect was estimated using the Digital Shoreline Analysis System (DSAS, Thieler et al., 2009). The DSAS has been successfully implemented in previous studies (e.g., Weserasingha and Ratnayake, 2022) and allows the shoreline retreat/advance to be quantified.

4. Results

4.1. Oceanic drivers: waves and sediment transport

4.1.1. Validation with in situ information

Seasonal variability of wave conditions and mean sea level are shown in Fig. 3. Wave energy shows maximum values during winter months associated with the *Nortes*' season, whereas the lowest energy levels occurred during the summer (Fig. 3a). The interannual variability is more important during the storm season, which might be related to climate variability (Medellín and Torres-Freyermuth, 2019). The peak wave period shows a similar variability. Long wave periods associated with swell waves occurred during the *Nortes*' season

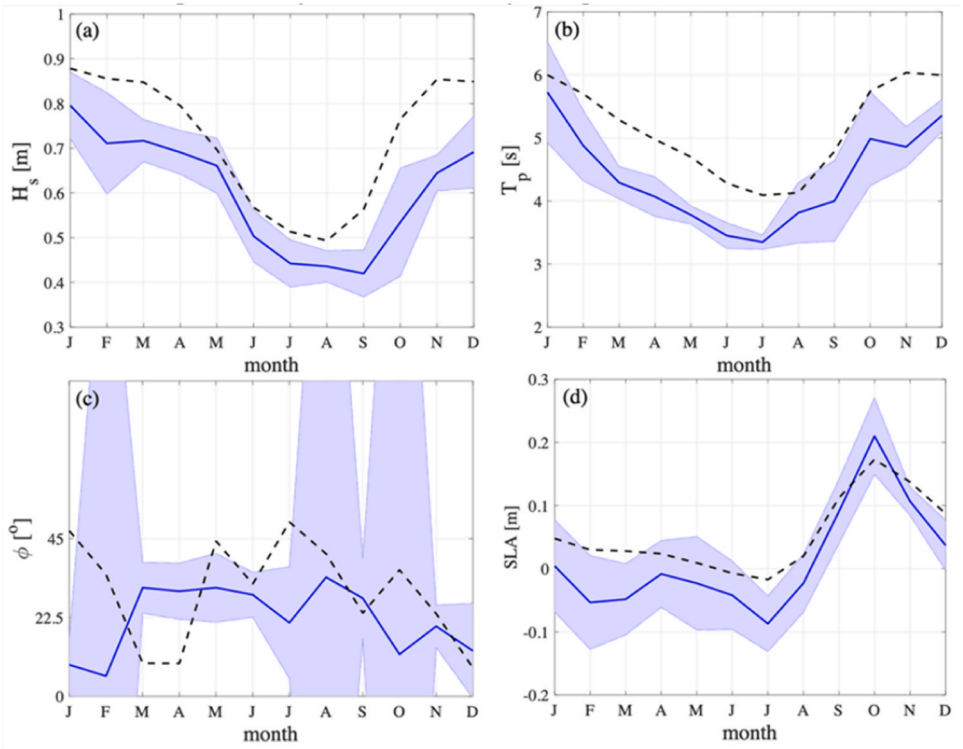

Fig. 3. Multi-annual monthly mean of (a-c) wave parameters and (d) water levels (monthly mode for the case of wave direction), where the shaded area represents ± one standard deviation of the monthly mean measurements (solid blue line). The dashed line in (a-c) represents the ERA5 and (d) AVISO+ estimates.

(October-February), whereas short wave periods due to sea breezes dominate the spring-summer. Sea breezes and trade winds induced waves from the NE (Fig. 1b); hence the average mode of measured wave direction is close to 30° from March to September. However, winter storms come from the N-NW; hence the mean of the wave direction mode changes to the NNE during the storm season (Fig. 3c). Wave reanalysis overpredict the measured significant wave height (see dashed line in Fig. 3a) and peak wave period (Fig. 3b), whereas the direction is quite consistent with NE wave observations, although it failed to describe the mean wave direction during January and February (Fig. 3c).

The altimetry information was validated with the tide gauge data in Sisal (Fig. 3d). The altimetry data reproduced the seasonal changes in the mean sea level (e.g., Zavala-Hidalgo et al., 2003), with a maximum mean sea level during October-November and minimum in July-August.

4.1.2. Alongshore transport

Alongshore sediment transport is very persistent in the study area due to the high-incidence angle short period waves associated with local winds (i.e., sea breezes). The net alongshore transport was computed for the 2015–2021 period as a function of the shoreline orientation (Fig. 4). The interannual variability, estimated by the standard deviation of annual Q_s, can be significant for shoreline orientations within the study area. The shoreline orientations vary from -11^o in Sisal and Progreso to -72^o in Celestún. The minimum (50,000 m^3/year) and maximum (85,000 m^3/year) Q_s were estimated at Celestún and El Palmar, respectively. In Punta Piedra and El Palmar both NE and NNW waves can drive westward alongshore transport due to their shoreline orientation.

4.2. Shoreline evolution

4.2.1. Satellite-derived shoreline validation

The shoreline position algorithm was validated with high-resolution in situ measurements acquired in Sisal since 2015. Fig. 5 shows the shoreline evolution at four transects located east of the port of Sisal (Fig. 1c). The satellite-derived shoreline position estimated seasonal changes (annual variability) and long-term trends (slope in the time series). At some locations (e.g., P20), the remote sensing information also predicted short-term oscillations, whereas there are larger differences at other locations. The latter can be ascribed to the beach slope, making the method more sensitive to tidal oscillations for transects located away from the structures which presents a milder slope.

Remote sensing was also compared against shoreline changes measured in the presence of temporal anthropogenic perturbations. A low-crested impermeable detached breakwater, made of sand-filled geotextile, was deployed at Punta San Miguel (Figs. 1b and 1d) in Summer 2017. High-resolution field observations were undertaken for 11 months using a differential GPS (Torres-Freyermuth et al., 2019). The structure induced significant changes in the shoreline position, promoting a shoreline advance on the lee-side of the structure of up to 60-m. A tombolo was generated, and the structure was partially removed due to the adverse effects at downstream locations (Torres-Freyermuth et al., 2019). The remote sensing information was compared with in situ measurements in Fig. 6, showing a satisfactory agreement. Moreover, the Sentinel-2 information allows us to analyze the shoreline evolution following the total removal of the structure when in situ measurements were no longer acquired (Fig. 6). It is noticed that the shoreline position on the lee-side of the structure moved further landward than the initial condition (i.e., 2016). These results confirm the remote sensing data capability to capture the shoreline response to external perturbations such as coastal structures.

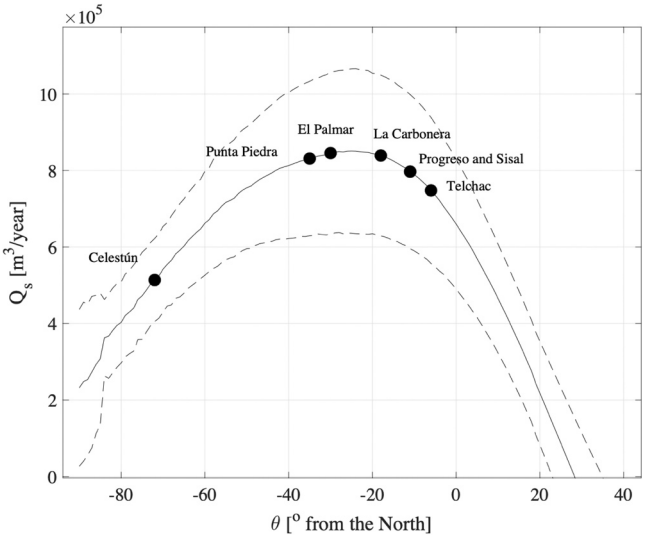

Fig. 4. Net alongshore sediment transport as a function of shoreline orientation. The circles represent selected sites along the study area.

4.2.2. Shoreline evolution: long-term trends

Satellite imagery from Landsat-5 and Sentinel-2 was employed to extract the shoreline position along the study area. Landsat (1985–2001) was employed to assess shoreline changes following the harbor's construction in the 1980s and Sentinel-2 to evaluate more recent changes influenced by coastal development and interannual changes. The analysis considers the transects between Celestún and Telchac (Fig. 1b). For the 1985–2001 period, the largest accretion occurred on the east side of Sisal, Yucalpeten, and Telchac harbors. On the other hand, the largest erosion occurred west of the ports of Chuburná and Sisal. The analysis shows that 44% of the transects presented erosion, whereas 31% presented accretion. This suggests that approximately 25% of the shoreline in the study area remained stable during this period.

The results of the analysis with a higher spatial and temporal resolution, using Sentinel-2 (2016–2022) at selected locations, are shown in Fig. 7. At a pristine area, located between the ports of Celestún and Sisal, a pattern of erosion-accretion is observed (Fig. 7a). A similar pattern in this area was obtained from the analysis of Landsat 5 images (not shown). Shoreline change estimates near the ports of Sisal present high shoreline accretion (erosion) rates to the east (west) of the ports (Fig. 7b). This is consistent with the impact of ports on beaches due to the net alongshore sediment transport from east to west in this region (Franklin et al., 2021). Significant erosion is also estimated downdrift of the Carbonera lagoon located between Sisal and Chuburná Harbor (Fig. 7c). Erosion extended for a few kilometers west of the Progreso Pier between the Yucalpeten and Chuburná Harbors (Fig. 7d). It is worth noticing that erosion was also present along the pristine coast of the natural reserve of El Palmar located between the ports of Celestún and Sisal.

The shoreline analysis for 2016–2022 suggests an increase in the downstream influence of the ports of Celestún and Telchac, changing from stable or accretion to erosion rates. The largest erosion occurred west of the Carbonera lagoon due to the alongshore growth of the sand spit, likely retaining the sand feeding the downdrift beach. The shoreline analysis using Sentinel-2 shows that 51% of the transects presented erosion, whereas 28% presented accretion. This suggests an increase (decrease) in shoreline erosion (accretion) during the last decade.

The results were compared against the shoreline trends inferred from numerical model results based on the potential littoral transport along the coast by Appendini et al. (2012). Satellite results were averaged along each polygon in the analysis of Appendini et al. (2012) to determine erosive, accretive, or stable conditions. Stable sections occurred when the percentage difference between erosive and accretive transects at each polygon was no larger than 10%. Fig. 8 compares the analysis by Appendini et al. (2012) and the satellite-derived results. Agreement between the two approaches is found at some locations. However, significantly more erosion was observed from the satellite-derived

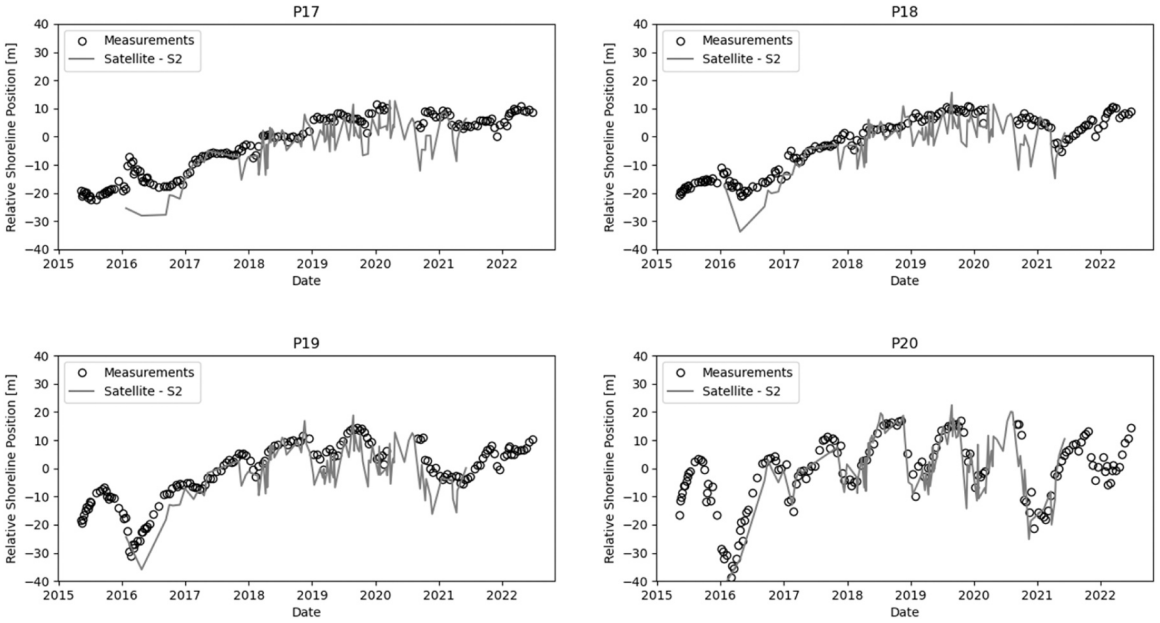

Fig. 5. Shoreline evolution at selected transects in Sisal, Yucatán (DGPS: open circles; Sentinel 2: solid line). See Fig. 1c for the location of the transects.

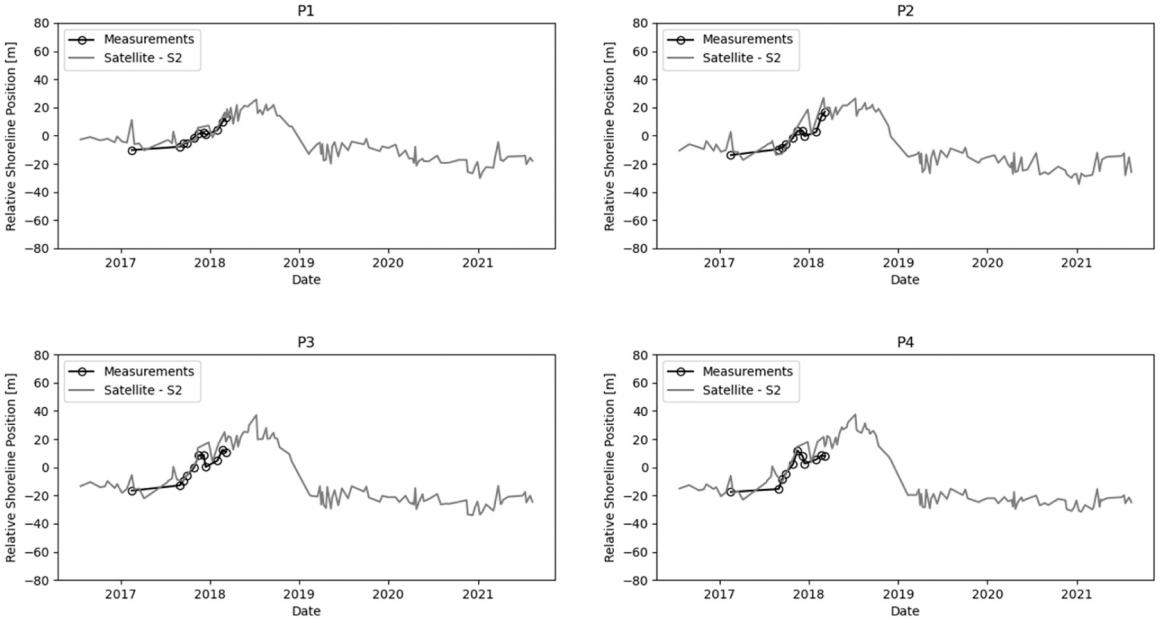

Fig. 6. Shoreline position changes at different alongshore locations in the vicinity of a low-crested detached breakwater in San Miguel, Yucatán (DGPS: open circles; Sentinel 2: solid line). See Fig. 1d for the location of the transects.

information. The work from Appendini et al. (2012) obtains the shoreline trends based on potential longshore transport gradients without considering the presence of structures. As such, the higher erosion trend found in this study compared to Appendini et al. (2012) is expected, particularly the largest differences found in the vicinity of the ports.

4.2.3. *Interannual shoreline variability*

A time stack of the shoreline position change along a 6-km stretch of coast in El Palmar suggests that the accretion/erosion pattern propagates toward the west (Fig. 9). The velocity of this shoreline perturbation propagation can be readily estimated with the slope of the accretion pattern in Fig. 9, which is approximately 300 m/year. A Principal Component Analysis (PCA) was also employed to estimate the characteristic wavelength of the sand wave. On one hand, the first spatial mode $e_1(y)$ (Fig. 10a), which contains 76% of the variance, shows a wavelength of approximately 2000 m (crests at 1000 m, 3000 m, and 5000 m). The first temporal mode $c_1(t)$ shows a sustained growth with time. On the other hand, the second mode (variance of 13%) is associated with the initial accretion-erosion pattern, where the crests are located near x = 2000 m, x = 4000 m, and x = 6000 m (Fig. 10c). The temporal mode suggests a reduction in this pattern over time. It is worth mentioning that the PCA is limited to stationary processes. The analysis suggests that interannual variability of shoreline position on the $O(10)$ m can dominate shoreline dynamics at certain locations of the study area.

4.2.4. *Seasonal shoreline variability*

The seasonal changes can be investigated with satellite-derived

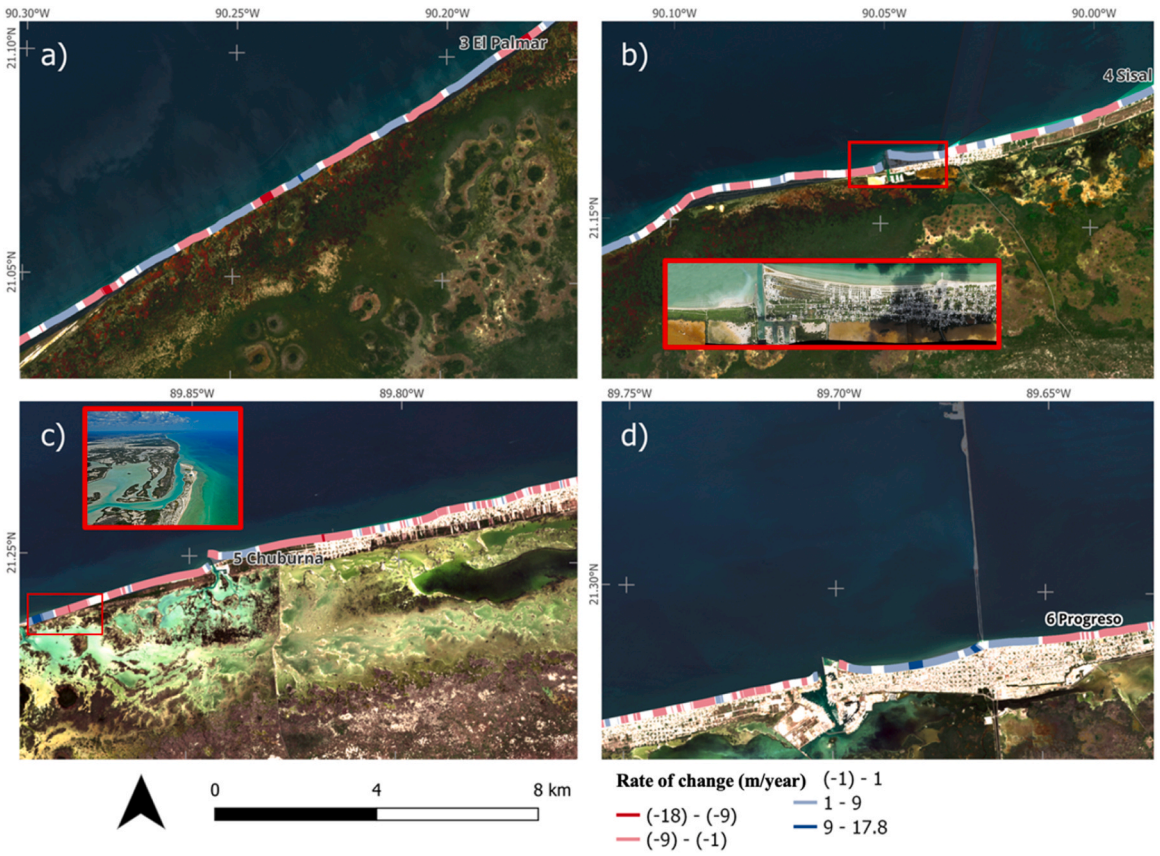

Fig. 7. Shoreline rate of change along the study area with focus on: (a) pristine area, (b) port of Sisal, (c) Carbonera lagoon and (d) Progreso-Chelem, Yucatan. Aerial pictures of La Carbonera and Sisal courtesy of aerozoom.mx.

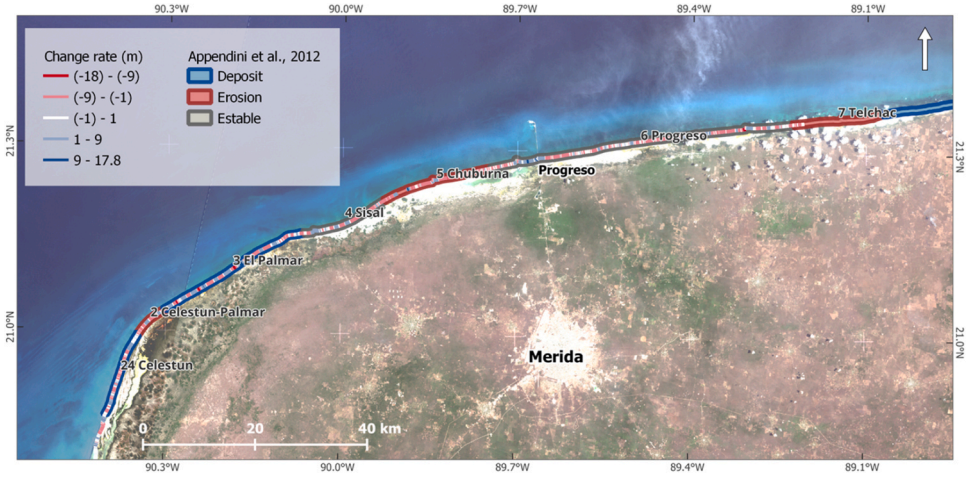

Fig. 8. Shoreline evolution as predicted by potential sediment transport gradients in Appendini et al. (2012) (outlines) and estimated from Sentinel-2 images (cross-shore transects).

shoreline information. The beach was analyzed at Sisal where the seasonal changes have been characterized with in situ information by Medellín and Torres-Freyermuth (2019). PCA was conducted along a 2-km stretch of coast covering the beach survey profiles (Fig. 1c). The first PCA spatial mode shows positive values, with the largest near the harbor, decreasing toward the pier (Fig. 11a). This is consistent with the sediment impoundment observed at this beach. The temporal evolution shows an increasing trend with some seasonal variability (Fig. 11b). The second spatial eigenfunctions of the second mode are consistent with the one obtained from in situ observations (Fig. 11a in Medellín and Torres-Freyermuth, 2019). Positive values are observed near the coastal structures with nodal points in between (Fig. 11c). This second mode was ascribed to beach rotation, which presents a cyclicity as depicted by the second temporal mode (Fig. 11d). Notice the abnormal seasonal variability in the shoreline occurring during the active 2020 hurricane season (Fig. 11d).

5. Discussion

The alternating erosion/accretion patterns at pristine locations along

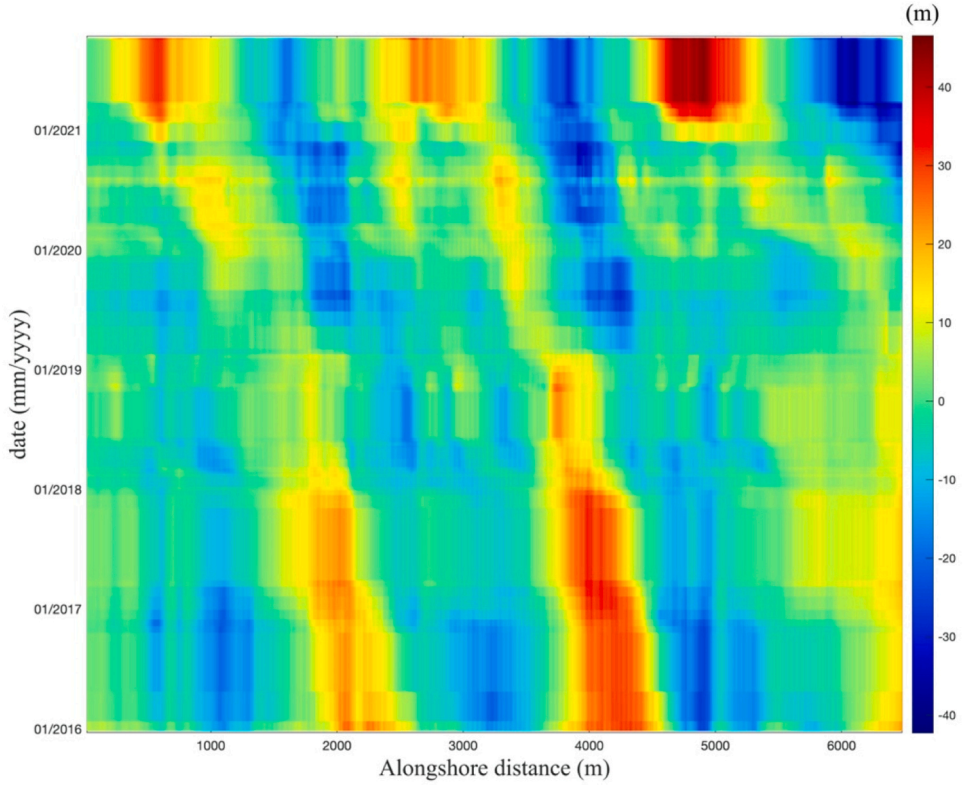

Fig. 9. Time stack of the shoreline change estimated from the Sentinel-2 images for the period of 2016–2021 at El Palmar.

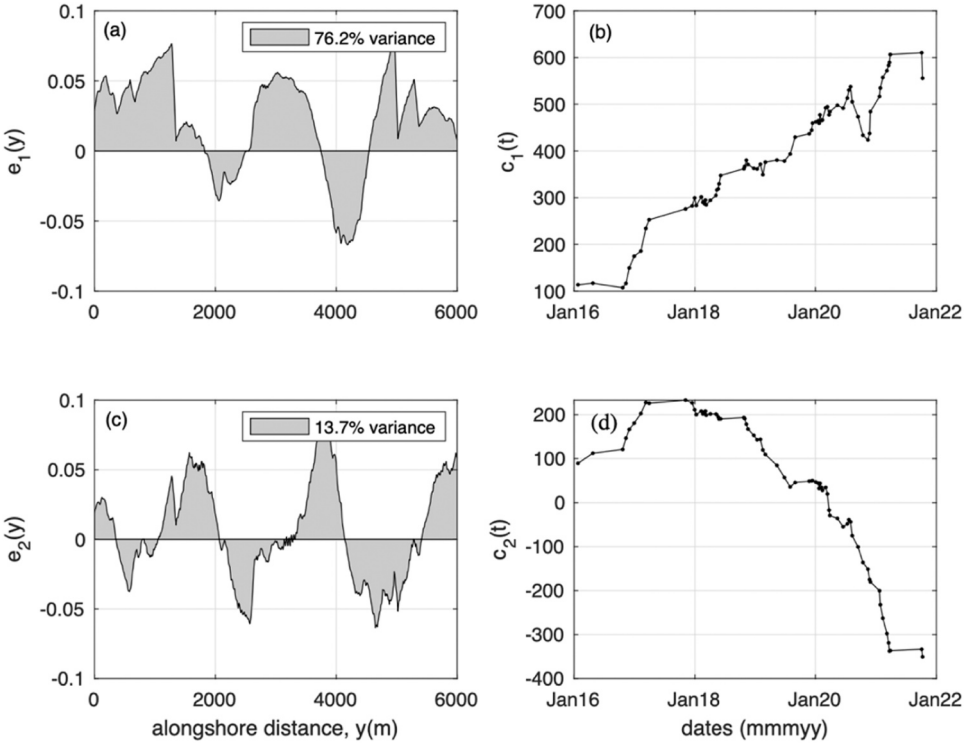

Fig. 10. First (a-b) and second (c-d) spatial and temporal modes of the shoreline position at El Palmar.

the northern Yucatan coast (e.g., see Fig. 7a), were previously reported by Ruiz-Beltran et al. (2019). However, a plausible explanation for the physical mechanisms driving such changes was not provided. The PCA at pristine locations suggests the presence of sand waves, which have been observed at many locations worldwide. Different generation mechanisms have been described in the literature, including the erosion downdrift of a structure (Inman and Brush, 1973), welding of the inner bar to the shoreline (Stewart and Davidson-Arnott, 1988), input of large

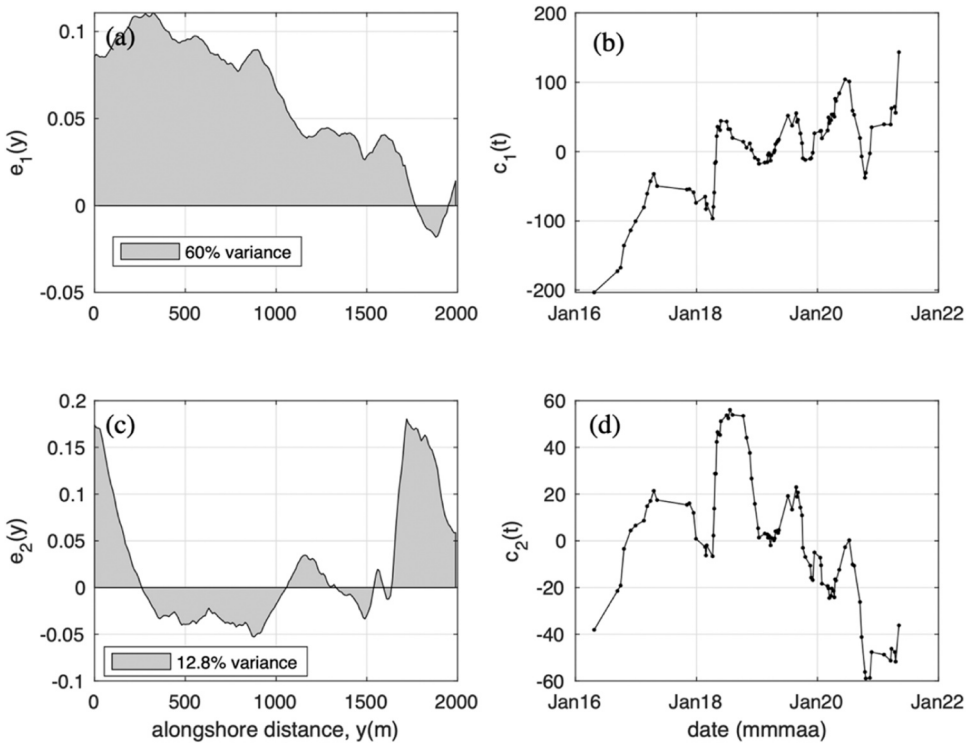

Fig. 11. First (a-b) and second (c-d) spatial and temporal modes of the shoreline position at Sisal beach. The alongshore distance is given with respect to Sisal Harbor.

amount of sediment to the beach (Warrick et al., 2023), high-angle (Ashton et al., 2001; Falqués and Calvete, 2005) and low-angle wave instability (Idier et al., 2011).

In this work, these morphological features present spatial scales (2–5 km) and migration rates (100–300 m/year) (see Section 4.2.3) that are consistent with previous observations (Guillen et al., 1999). Sand wave generation was clearly observed at Punta Piedra, a stretch of coast where the coastline changes orientation (Fig. 12). Coastline and bathymetric curvature induced local variability in the longshore sediment transport (e.g., Inman and Jenkins, 2018) that can promote sediment deposition. Fig. 12a shows the change in coastline orientation at Punta Piedra, from WNW-ESE to NE-SW, that causes a gradient in the alongshore sediment transport due to NE persistent wave conditions (see wave rose in Fig. 1). This change in orientation promotes the formation of a spit that is attached downdrift, creating a runnel that can be eventually infilled by wave overwash events (Stewart and Davidson-Arnott, 1988). The sand waves propagate downdrift, and their migration is clearly observed in the timestack of shoreline change (i.e., Fig. 9).

Sand waves in the study area could also be induced by the downdrift erosion of coastal structures (Inman and Brush, 1973) and the subsequent removal of such structures. Fig. 13a shows the shoreline response due to the presence of two low-crested detached breakwaters, made of geotextile filled with sand, installed in 2017 at San Bruno. These structures induced significant downdrift erosion (Fig. 13a). The structures were removed months later and caused an accretion/erosion propagating wave travelling downdrift at 290 m/year (slope of the dashed line in Fig. 13b).

6. Conclusions

We investigate satellite-derived shoreline changes on a 150-km stretch of coast along the northern Yucatan coast. Satellite and reanalysis information were validated with in situ data. Long-term analysis suggests that 50% of the coast is retreating, whereas 30% is accreting, and 20% remains stable. Shoreline changes are associated with the persistent net alongshore sediment transport toward the west in combination with natural and anthropogenic perturbations. The main anthropogenic perturbations are associated with coastal infrastructure (Progreso 6 km long Pier and sheltered harbors) and coastal structures

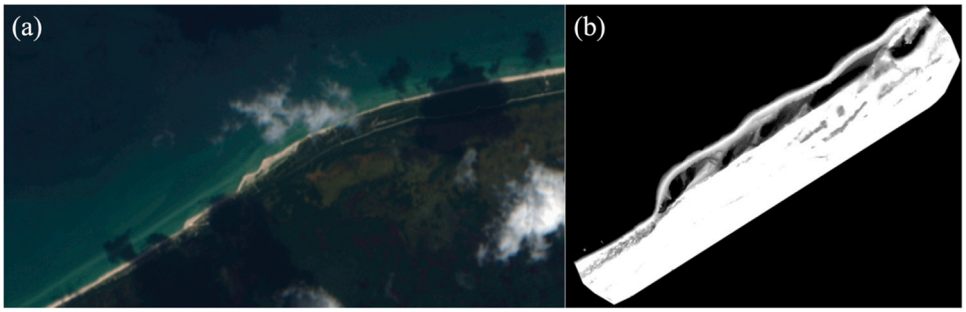

Fig. 12. (a) Satellite images from Sentinel 2 (October 14, 2021) showing formation of a longshore sand wave at Punta Piedra (northwestern Yucatan coast) consistent with the nearshore bar attachment model by Stewart and Davidson-Arnott (1988). (b) A digital terrain model from this study area obtained in December 2022 showing the sand spits and runnels.

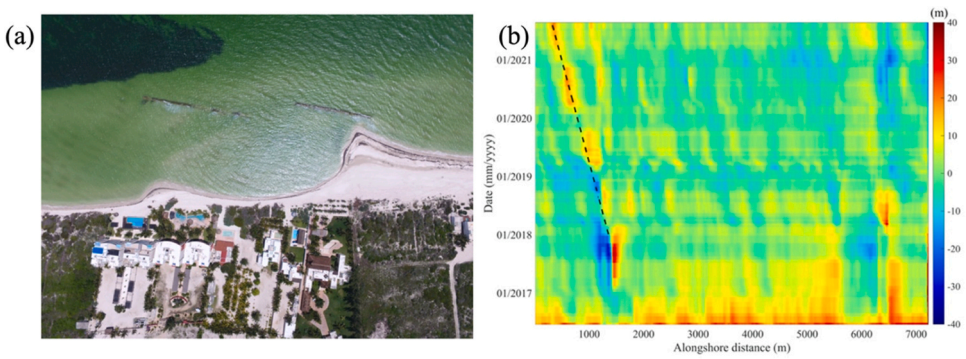

Fig. 13. (a) Aerial photo of shoreline response to the presence of low-crested detached breakwaters at San Bruno. (b) Spatial and temporal evolution of the shoreline position showing the generation of the disturbance and subsequent propagation after the structure removal. The slope of the dashed line represents the migration velocity of the sand wave.

(groins and detached breakwaters) inducing downdrift erosion from 500 m to 10 km. Natural perturbations are mainly associated with changes in shoreline orientation that induce sediment transport gradients. Furthermore, a coastal lagoon also affected beaches located downdrift owing to the growth of sand spits, producing a similar impact at downdrift beaches than harbors. Natural and anthropogenic perturbations can trigger propagating sand waves that can cause erosion/accretion cycles with a period of approximately five years. These sand waves generate up to 40 m shoreline cross-shore oscillations and present a 2000 m characteristic wave length. The sand waves travel due to advection diffusion mechanisms associated with the highly oblique wave direction in this region and propagate at a rate of 300 m/year. These features can be found in pristine and urbanized locations and play an important role in shoreline dynamics along the northern Yucatan coast. The propagation of sand waves might trigger the implementation of inadequate mitigation measures, such as breakwaters and groins, that do not consider the cyclic high erosion rates associated with their passage, exacerbating the erosion problem. Therefore, studying sand waves growth, migration, and destruction in this region is warranted.

CRediT authorship contribution statement

Alec Torres-Freyermuth: Conceptualization, Methodology, Investigation, Formal analysis, Visualization, Writing - original draft, Supervision. **Eduardo López-Ramade:** Software, Investigation, Visualization, Formal analysis, Writing - review & editing. **Gabriela Medellín:** Methodology, Data curation, Formal analysis, Investigation, Visualization, Writing - review & editing. **Jaime A. Arriaga**: Software, Formal analysis, Investigation, Writing - review & editing. **Gemma L. Franklin:** Data curation, Formal analysis, Writing - review & editing. **Paulo Salles:** Conceptualization, Methodology, Writing - review & editing, Funding acquisition. **Abigail Uribe:** Data curation, Formal analysis, Visualization, Writing - review & editing. Christian **M. Appendini:** Conceptualization, Methodology, Writing - review & editing.

Declaration of Competing Interest

The authors declare that they have no known competing financial interests or personal relationships that could have appeared to influence the work reported in this paper.

Data availability

The computed shoreline trends from Landsat 5, Landsat 8, and Sentinel-2 can be visualize on a Google Earth using the kml file https://www.dropbox.com/s/8pok6qgc0ow04n5/Cambio%20l%C3%ADnea%20costa.kmz?dl=0.

Acknowledgements

Field support was provided by Juan Alberto Gómez Liera, Camilo Sergio Rendón Valdez, José López González and Jorge Alejandro Kurzcyn Robles. Additional IT technical support was provided by Gonzalo Uriel Martín Ruiz. Financial support was provided Ducks Unlimited de México A.C., DGAPA-UNAM PAPIIT (IA101422 and IV300123), and UNAM Instituto de Ingeniería (GII-3117). We acknowledge Copernicus programme for making satellite and reanalysis information available. Also, we thank Kilian Vos for the development of the open-source remote sensing tool CoastSat which was fundamental for conducting this research. Comments from Prof. Amila Sandaruwan Ratnayake and an anonymous reviewer significantly improve the manuscript.

References

Almar, R., Boucharel, J., Graffin, M., Abessolo, G.O., Thoumyre, G., Papa, F., Ranasinghe, R., Montano, J., Bergsma, E.W.J., Baba, M.W., Jin, F.-F., 2023. Influence of El Niño on the variability of global shoreline position. Nat. Commun. 14, 3133.

Amalan, K., Ratnayake, A.S., Ratnayake, N.P., Weththasinghe, S.M., Dushyantha, N., Lakmali, N., Prmasiri, R., 2018. Influence of nearshore sediment dynamics on the distribution of heavy mineral placer deposits in Sri Lanka. Environ. Earth Sci. 77, 737.

Appendini, C.M., Salles, P., Mendoza, E.T., López, J., Torres-Freyermuth, A., 2012. Longshore sediment transport on the Northern Coast of the Yucatan Peninsula. J. Coast. Res. 28 (6), 1404–1417. ISSN 0749-0208.

Ashton, A., Murray, A.B., Arnault, O., 2001. Formation of coastline features by large-scale instabilities induced by high-angle waves. Nature 414, 296–300.

Ashton, A.D., Murray, A.B., 2006. High-angle wave instability and emergent shoreline shapes: 1. Modeling of sandwaves, flying spits, and capes. J. Geophys. Res. 111, F04011. https://doi.org/10.1029/2005JF000422.

Aubrey, D.G., 1979. Seasonal patterns of onshore/offshore sediment movement. J. Geophys. Res. 84 (C10), 6347–6354.

Barnard, P.L., Hoover, D., Hubbard, D.M., Snyder, A., Ludka, B.C., Allan, J., Kaminsky, G. M., Ruggiero, P., Gallien, T.W., Gabel, L., McCandless, D., Weiner, H.M., Cohn, N., Anderson, D.L., Serafin, K.A., 2017. Extreme oceanographic forcing and coastal response due to the 2015–2016 El Niño. Nat. Commun. 8 (14365) (Doi:10.1038).

Castelle, B., Masselink, G., Scott, T., Stokes, C., Konstantinuou, A., Marieu, V., Bujan, S., 2021. Satellite-derived shoreline detection at a high-energy meso-macrotidal beach. Geomorphology 383, 107707.

CoastSat: https://github.com/kvos/CoastSat.

Coco, G., Murray, A.B., 2007. Patterns in the sand: from forcing templates to self-organization. Geomorphology 91, 271–290.

Davidson-Arnott, R.G.D., Van Heyningen, A.G., 2003. Migration and sedimentology of longshore sandwaves, Long Point, Lake Erie, Canada. Sedimentology 50, 1123–1137. https://doi.org/10.1046/j.1365-3091.2003.00597.x.

De Winter, R.C., Gongriep, F., Ruessink, B.G., 2014. Observations and modeling of alongshore variability in dune erosion at Egmond aan Zee, the Netherlands. Coast. Eng. 99, 167–175.

Falqués, A., 2006. Wave driven alongshore sediment transport and stability of the Dutch coastline. Coast. Eng. 53, 243–254.

Falqués, A., Calvete, D., 2005. Large scale dynamics of sandy coastlines. Diffusivity and instability. J. Geophys. Res. 110, C03007. https://doi.org/10.1029/2004JC002587.

Figueroa-Espinoza, B., Salles, P., Zavala, J., 2014. On the wind power potential in the northwest of the Yucatan Peninsula in Mexico. Atmósfera 27 (1), 77–89. ISSN: 0187-6236.

Franklin, G.L., Medellín, G., Appendini, C.M., Gómez, J.A., Torres-Freyermuth, A., López González, J., Ruiz-Salcines, P., 2021. Impact of port development on the northern Yucatan Peninsula coastline. Reg. Stud. Mar. Sci. 45, 101835 https://doi.org/10.1016/j.rsma.2021.101835.

Gallagher, E.L., Elgar, S., Guza, R.T., 1998. Observations of sand bar evolution on a natural beach. J. Geophys. Res. 103 (C2), 3203–3215.

Garcia-Rubio, G., Huntley, D., Russell, P., 2015. Evaluating shoreline identification using optical satellite images. Mar. Geol. 359, 96–105 https://doi.org/10.1016/j.margeo.2014.11.002.

Guillen, J., Stive, M.J.F., Capobianco, M., 1999. Shoreline evolution of the Holland Coast on a decadal scale. Earth Surf. Process. Landf. 24, 517–536.

Gunasinghe, G.P., Ratnayake, N.P., Ratnayake, A.S., Samaradivakara, G.V.I., Dushyantha, N.P., Jayaratne, R., Dinusha, K.A., Silva, A., 2022. Monsoon-driven geomorphological changes along the West Coast of Sri Lanka: a combined approach utilizing 'CoastSat' and Google Earth Engine. Ocean Sci. J. 57, 475–492. https://doi.org/10.1007/s12601-022-00081-z.

Hansen, J.E., Barnard, P.L., 2010. Sub-weekly to interannual variability of a high-energy shoreline. Coast. Eng. 57, 959–972.

Harley, M.D., Turner, I.L., Short, A.D., Ranasinghe, R., 2011. A reevaluation of coastal embayment rotation: the dominance of cross-shore versus alongshore sediment transport processes, Collaroy-Narrabeen Beach, southeast Australia. J. Geophys. Res. 116, F04033.

Harley, M.D., Turner, I.L., Short, A.D., 2015. New insights into embayed beach rotation: the importance of wave exposure and cross-shore processes. J. Geophys. Res. Earth Surf.,120 1470–1484. https://doi.org/10.1002/2014JF003390.

Harley, M.D., Masselink, G., Ruiz de Alegría-Arzaburu, A., Valiente, N.G., Scott, T., 2022. Single extreme storm sequence can offset decades of shoreline retreat projected to result from sea-level rise. Commun. Earth Environ. 3, 112.

Hoefel, F., Elgar, S., 2003. Wave-induced sediment transport and sandbar migration. Science 299, 1885–1887.

Idier, D., Falqués, A., Ruessink, B.G., Garnier, R., 2011. Shoreline instability under low-angle wave incidence. J. Geophys. Res. 116, F04031. https://doi.org/10.1029/2010JF001894.

INEGI, 2001. Uso del suelo y vegetación, escala 1:250000, serie II (continuo nacional), escala: 1:250000. Dirección General de Geografía. Instituto Nacional de Estadística y Geografía. Instituto Nacional de Estadística y Geografía (INEGI), Aguascalientes, Ags., México.

INEGI, 2021. Conjunto de Datos Vectoriales de Uso de Suelo y Vegetación. Escala 1:250 000, Serie VII. Conjunto Nacional, escala: 1:250 000. edición: 1. Instituto Nacional de Estadística y Geografía, Aguascalientes, México.

Inman, D.L., Bagnold, R.A., 1963. Littoral processes. In: Hill, M.N. (Ed.), The Sea, Volume 3, The Earth Beneath The Sea. Wiley, New York/London, pp. 529–553.

Inman, D.L., Brush, B.M., 1973. The coastal challenge. Science 181, 20–32.

Inman, D.L., Jenkins, S.A., 2018. Accretion and Erosion Waves on Beaches. In: Finkl, C., Makowski, C. (Eds.), Encyclopedia of Earth Sciences Series, Encyclopedia of Coastal Science. Springer, Cham. https://doi.org/10.1007/978-3-319-48657-4_1-2.

Komar, P.D., 1998. Beach Processes and Sedimentation, 2nd edition. Prentice-Hall, Englewood-Cliffs.

Medellin, G., Torres-Freyermuth, A., Tomasicchio, G.R., Francone, A., Tereszkiewicz, P. A., Lusito, L., Palemón-Arcos, L., López, J., 2018. Field and numerical study of resistance and resilience on a sea breeze dominated beach in Yucatan (Mexico). Water 10, 1806. https://doi.org/10.3390/w10121806.

Medellín, G., Torres-Freyermuth, A., 2019. Morphodynamics along a micro-tidal sea breeze dominated beach in the vicinity of coastal structures. Mar. Geol. 417, 106013.

Medellín, G., Medina, R., Falqués, A., González, M., 2008. Coastline sand waves on a low-energy beach at "El Puntal spit", Spain. Mar. Geol. 250, 143–156.

Mendoza, E.T., Trejo-Rangel, M.A., Salles, P., Appendini, C.M., Lopez-Gonzalez, J., Torres-Freyermuth, A., 2013. Storm characterization and coastal vulnerability in the Yucatan Peninsula. ISSN 0749-0208 J. Coast. Res. (Special Issue No. 65), 790–795. https://doi.org/10.2112/SI65-134.1.

Meyer-Arendt, K.J., 1987. Recreational landscape evolution along the north Yucatan coast. Conf. Lat. Am. Geogr. 13, 45–50.

Meyer-Arendt, K.J., 1993. Shoreline changes along the north Yucatan coast. In: Laska, S. and Puffer, A. (eds.), Coastlines of the Gulf of Mexico, Coastlines of the World Series, gen. ed. O. Magoon (ASCE, NY). Proceedings of the Eight Symposium on Coastal and Ocean Management (Coastal Zone '93), New Orleans, pp. 103–117.

Mortlock, T.R., Goodwin, I.D., 2016. Impacts of enhanced central pacific ENSO on wave climate and headland-bay beach morphology. Cont. Shelf Res. 120, 14–25.

Neal, T.C., Appendini, C.M., Rankey, E.C., 2021. Hydrodynamic influences on sedimentology and geomorphology of nearshore parts of carbonate ramps: Holocene, NE Yucatán Shelf, Mexico. J. Sediment. Res. 91 (10), 1040–1066.

Ngcamu, B.S., 2023. Climate change effects on vulnerable populations in the Global South: a systematic review. Nat. Hazards 118, 977–991. https://doi.org/10.1007/s11069-023-06070-2.

Nidhinarangkoon, P., Ritphring, S., Kino, K., Oki, T., 2023. Shoreline changes from erosion and sea level rise with coastal management in Phuket, Thailand. J. Mar. Sci. Eng. 11 (5).

Ocaña, F.A., Olmos-García, R.E., de Jesús-Carrillo, R.M., Noreña-Barroso, E., Guerra-Castro, E., 2023. Spatiotemporal patterns of macrophyte subsides to sandy beaches of Yucatán, Mexico. Reg. Stud. Mar. Sci. 63, 10297.

Odériz, I., Silva, R., Mortlock, T.R., Mori, N., 2020. El Niño-Southern Oscillation Impacts on Global Wave Climate and Potential Coastal Hazards. J. Geophys. Res. 125 (12), e2020JC016464.

Ojeda, E., Guillen, J., 2008. Shoreline dynamics and beach rotation of artificial embayed beaches. Mar. Geol. 253, 51–62.

Paré, L., Fraga, J., 1994. La costa de Yucatán: Desarrollo y vulnerabilidad ambiental. In: Gordon, S. (Ed.), Cuadernos de Investigación, Instituto de Investigaciones Sociales, Universidad Nacional Autónoma de México.

Pattiaratchi, C., Olsson, D., Hetzel, Y., Lowe, R., 2009. Wave driven circulation patterns in the lee of groynes. Cont. Shelf Res. 29 (16), 1961–1974.

Ranasinghe, R., 2016. Assesing climate change impacts on open sand coast: a review. Earth-Sci. Rev. 160 (9), 320–332.

Ranasinghe, R., Callaghan, D., Stive, M.J.F., 2012. Estimating coastal recession due to sea level rise: beyond the bruun rule. Clim. Change 110 (3), 561–574. https://doi.org/10.1007/s10584-011-0107-8.

Ratnayake, N.P., Ratnayake, A.S., Keegle, P.V., et al., 2018. An analysis of beach profile changes subsequent to the Colombo Harbor Expansion Project, Sri Lanka. Environ. Earth Sci. 77, 24.

Ranasinghe, R., Turner, I.L., 2006. Shoreline response to submerged structures: a review. Coast. Eng. 53 (1), 65–79.

Ratnayake, N.P., Ratnayake, A.S., Azoor, R.M., et al., 2019. Erosion processes driven by monsoon events after a beach nourishment and breakwater construction at Uswetakeiyawa beach, Sri Lanka. SN Appl. Sci. 1, 52.

Reding, P.J., 1992. The Central American Cold Surge: an observational analysis of the deep southward penetration of North American cold fronts, MSc. Thesis, Tex. AM Univ. 192.

Roberts Briggs, T., Figlus, J., Torres-Freyermuth, A., Puleo, J., Warren, W., Alrushaid, T., 2020. Variability in onshore sediment transport on a natural beach during a Central American Cold Surge Event. J. Coast. Res. 36 (3), 487–497.

Ruiz de Alegria-Arzaburu, A., Masselink, G., 2010. Storm response and beach rotation on a gravel beach. Mar. Geol. 278, 77–99.

Ruiz-Beltran, A.P., Astorga-Moar, A., Salles, P., Appendini, C.M., 2019. Short-term shoreline trend detection patterns using SPOT-5 image fusion in the Northwest Yucatan, Mexico. Estuaries Coasts 42 (7), 1761–1773.

Sallenger, A.H., Holman, R.A., Birkemeier, W.A., 1985. Storm-induced response of a nearshore-bar system. Mar. Geol. 64 (Issues 3–4), 237–257.

Stewart, C.J., Davidson-Arnott, R.G.D., 1988. Morphology, formation and migration of longshore sandwaves; Long Point, Lake Erie. Can. Mar. Geol. 81, 63–77.

Thieler, E.R., Himmelstoss, E.A., Zichichi, J.L., Ergul, A., 2009. Digital Shoreline Analysis System (DSAS) version 4.0- An ArcGIS extension for calculating shoreline change: U. S. Geological Survey Open-File Report 2008–1278. http://woodshole.er.usgs.gov/project-pages/dsas/.

Torres-Freyermuth, A., Medellín, G., Mendoza, E.T., Ojeda, E., Salles, P., 2019. Morphodynamic response to low-crested detached breakwaters on a sea breeze-dominated coast. Water 11, 635.

Turner, I.L., 2006. Discriminating modes of shoreline response to offshore-detached structures. J. Water Port. Coast Ocean Eng. 132 (3), 180–191. https://doi.org/10.1061/(asce)0733-950x(2006)132:3(180.

Turner, I.L., Harley, M.D., Almar, R., Bergsma, E.W.J., 2019. Satellite optical imagery in Coastal Engineering. Coast. Eng. 167, 103919.

Valle-Levinson, A., Mariño-Tapia, I., Enriquez, C., Waterhouse, A., 2011. Tidal variability of salinity and velocity fields related to intense point-source submarine groundwater discharges into the coastal ocean. Limnol. Oceanogr. 56 (4), 1213–1224.

Vidal-Ruiz, J.A., Ruiz de Alegría-Arzaburu, A., 2019. Variability of sandbar morphometrics over three seasonal cycles on a single-barred beach. Geomorphology 333, 61–72.

Vitousek, S., Vos, K., Splinter, K.D., Erikson, L., Barnard, P.L., 2023. A model integrating satellite-derived shoreline observations for predicting fine-scale shoreline response to waves and sea-level rise across large coastal regions. J. Geophys. Res.: Earth Surf. 128 (7).

Vos, K., Splinter, K.D., Darley, M.D., Simmons, J.A., Turner, I.L., 2019. CoastSat: A Google Earth Engine-enable Phyton toolkit to extract shorelines from publicly available satellite imagery. Environ. Model. Softw. 122, 104528.

Warrick, J.A., Vos, K., Buscombe, D., Ritchie, A.C., Curtis, J.A., 2023. A large sediment accretion wave along a Northern California littoral cell. J. Geophys. Res.: Earth Surf. 128 e2023JF007135.

Weserasingha, W.A.D.B., Ratnayake, A.S., 2022. Coastal landform changes on the east coast of Sri Lanka using remote sensing and geographic information system (GIS) techniques. Remote Sens. Appl.: Soc. Environ. Volume 26, 100763.

Westley, K., Nikolaus, J., Emrage, A., Flemming, N., Cooper, A., 2023. The impact of coastal erosion on the archaeology of the Cyrenaican coast of Eastern Libya. PLoS ONE Volume 18 (Issue 4).

Williams, H.F.L., 1999. Sand-spit erosion following interruption of longshore sediment transport: Shamrock Island, Texas. Environ. Geol. 37 (1–2).

Wright, L.D., Short, A.D., 1984. Morphodynamic variability of surf zones and beaches: a synthesis. Mar. Geol. 56, 93–118.

Zavala-Hidalgo, J., Morey, S.L., O'Brien, J.O., 2003. Seasonal circulation on the western shelf of the Gulf of Mexico using a high-resolution numerical model. J. Geophys. Res. 108, C12 108 (C12), 3389. https://doi.org/10.1029/2003JC001879.

Zenkovich, V.P., 1967. Processes of Coastal Development. Interscience Publishers, New York, p. 751.